

Research Paper

Evaluation of Elastic Settlement Behavior in Small-Strain Range of Cement-Treated Clayey Soil

M. A. Putera ¹, N. Yasufuku ², A. Alowaisy ³, R. Ishikura ⁴, J. G. Hussary ⁵, and A. Rifa'i ⁶

ARTICLE INFORMATION

Article history:

Received: 17 June, 2022

Received in revised form: 29 July, 2022

Accepted: 30 July, 2022

Publish on: 24 October, 2022

Keywords:

Elastic settlement

Curing Period

Cement content

Confining pressure

Dynamic loading

Small-strain



This work is licensed under a Creative Commons Attribution-NonCommercial 4.0 International License.

ABSTRACT

Indonesia is developing high-speed railway lines that are expected to connect the major cities. Along the railway, the lowland area is mainly comprised of clayey soil characterized by a high compressibility index and high water content, which causes soil settlement in the long term. Therefore, to reduce the potential of settlement, choosing a suitable railway structure, such as the ballastless track, is essential. Despite the track structure, the subsoil mechanical properties often require improvement to limit the railways' settlement. Using cement-treated soil, a combination technique was provided to protect the shallow ground and the ballastless track, effectively reducing the stress distribution during construction periods and maintaining low construction costs for developing countries. To assure longer serviceability, there is a high need for an accurate evaluation of the elastic settlement subjected to train loading. Therefore, this paper proposes an elastic settlement prediction model for cement-treated soils considering the curing period, cement content, and confining pressure within the small-strain ranges. The model optimizes the mixing ratio at a specific curing period, reflecting the wheel-base loading on the cement-treated soil layer. Moreover, a simple power formula to determine the initial mechanical properties of the cement-treated soils was proposed.

1. Introduction

Among other developing countries, Indonesia is developing its infrastructure, including a high-speed Railway (HSR) project (maximum speed of 300 km/h) that is expected to connect the Jakarta and Surabaya cities, extending for 700 km (JETRO, 2012). Along the railway,

the lowland area is mainly comprised of clayey soil characterized by a high compressibility index and high water content (Novico et al., 2022; Ranst et al., 2004). Such conditions impose significant geotechnical challenges, including lack of bearing capacity, stability loss, and significant volume changes causing differential settlement. Therefore, innovative and economic

¹ Doctoral Student, Geotechnical Engineering Laboratory, Department of Civil Engineering, Faculty of Engineering, Kyushu University, 744 Motoooka, Nishi-ku, Fukuoka 819-0395, JAPAN, muhammad.akmal.putera@gmail.com (Corresponding author)

² Professor, Geotechnical Engineering Laboratory, Department of Civil Engineering, Faculty of Engineering, Kyushu University, 744 Motoooka, Nishi-ku, Fukuoka 819-0395, JAPAN, yasufuku@civil.kyushu-u.ac.jp

³ Assistant Professor, Geotechnical Engineering Laboratory, Department of Civil Engineering, Faculty of Engineering, Kyushu University, 744 Motoooka, Nishi-ku, Fukuoka 819-0395, JAPAN, a.adel@civil.kyushu-u.ac.jp

⁴ Associate Professor, Geotechnical Engineering Laboratory, Department of Civil Engineering, Faculty of Engineering, Kyushu University, 744 Motoooka, Nishi-ku, Fukuoka 819-0395, JAPAN, ishikura@civil.kyushu-u.ac.jp

⁵ Doctoral Student, Geotechnical Engineering Laboratory, Department of Civil Engineering, Faculty of Engineering, Kyushu University, 744 Motoooka, Nishi-ku, Fukuoka 819-0395, JAPAN, jumanahusary@gmail.com

⁶ Associate Professor, Department of Civil and Environmental Engineering, Faculty of Engineering, Universitas Gadjah Mada, Yogyakarta 55281, INDONESIA, ahmad.rifai@ugm.ac.id

techniques are needed to ensure the safety of life and properties.

Generally, railway structures can be divided into ballasted and ballastless structures. The ballasted structures are heavyweight, costly to maintain, and characterized by high shear strength and low vertical settlement. On the other hand, the ballastless is lightweight, relatively cheaper to maintain, and efficient for sites experiencing differential settlement (Kumar and Singh, 2017). Therefore, ballastless structures are commonly utilized for HSR projects in lowlands (Kang, 2016; Kumar and Singh, 2017). Despite the track structure, the subsoil mechanical properties often require improvement to limit the railways' settlement. Several techniques are commonly used, such as superstructures (bridges and embankments), pile foundation, drained consolidation methods, deep soil mixing, and shallow stabilization. Due to the low cost, shallow stabilization is commonly practiced to prevent static and dynamic loading-induced settlement, especially in developing countries. Recently, the utilization of stabilized soil by substituting the cement content with granulated blast furnace slag and bamboo ash is assessed to reducing the potential settlement based on the pozzolanic reaction (Ikeagwuani et al., 2019). However, using the cement products, it more significantly shown reducing the potential settlement, especially of clayey soil with high compressibility index (Firoozi et al., 2017).

The total soil settlement is comprised of elastic and consolidation settlements (Das, 1985), while in practice, mainly the latter is considered. The maximum allowable settlement for HSR associated with the dynamic loading is ≤ 30 mm, while it is limited to 10 mm/year for the earthquake loading (Ando et al., 2021; Kanazawa and Tarumi, 2010). In the case of HSR, combining the ballastless structure with shallow cement stabilization might be inevitable, where especially during the construction and the early operational stages, the elastic settlement with time might be of significant importance. During the construction phase, the soil stiffness of the underlying soil increases gradually, causing a reduction in the elastic settlement. However, during the post-construction (operation phase), the dynamic loading associated with the train's passage induces mainly elastic settlement (Lazorenko et al., 2019; Pantelidis and Gravanis, 2020). Therefore, the initial stiffness and the determination of the small-strain mechanical parameters are vital for analyzing the behavior and predicting the elastic settlement in the long-term operation of the HSR (Atkinson, 2000; Fang and Daniels, 2006; Foye et al., 2008).

Numerous models were proposed to predict the elastic settlement of soil profiles. One of the most used is the

Boussinesq formula (Hu et al., 2016). The formula discusses the generalized elastic approach of shallow foundation, considering Young's modulus of the homogenous soil layer under uniform loading (Skempton and Bjerrum, 1957). Das and Ramana (2010) asserted the importance of estimating the maximum dynamic loading behavior, which can be obtained considering the load transmission to the substructure. Poulos and Davis (1968) and Mayne and Poulos (1999) proposed the influence factor in correlation with vertical displacement. It reflects the depth of interest in the substructure embedment or the substructure geometry below the ground. Horikoshi and Randolph, (1997) derived a substructure-soil stiffness ratio for a rectangular foundation equivalent to a circular one for predicting the elastic settlement under rectangular geometry. Razouki and Al-Zubaidy, (2010) reported the efficiency of reinforcing a specific layer thickness to reduce the elastic settlement. However, a comprehensive elastic settlement evaluation model for cement-treated soils subjected to dynamic loading that considers the thickness of the cement-treated layer is lacking.

This paper introduces a new elastic settlement prediction model for cement-treated clayey ground focusing on the small-strain range. The model considers low-stress dynamic loading associated with the train passage and correlates it to the soil layer thickness (confining pressure). A series of undrained triaxial tests equipped with proper small strain testing devices were conducted to investigate the small strain zone behavior.

2. Materials and Methodology

2.1 Materials: soil and cement content

In this study, the Ariake clay was used and collected around Ariake bay in the western part of Kyushu Island, Japan. The particle size distribution curve and the physical and mechanical properties of the Ariake clay are shown in **Fig.1** and **Table 1**, respectively. Based on the Japanese Geotechnical Society Standard (JGS 0051-2009), the Ariake clay is classified as cohesive soil with a high liquid limit (C.H.). The oedometer test was conducted to determine the compressibility index and the preconsolidated pressure. **Fig. 2** delineates the consolidation curve (e-log p curve), where the sample is overconsolidated.

Ordinary Portland Cement (OPC) was used as a binder material to enhance the Ariake clay mechanical properties. The chemical components of the Japanese OPC consist of the C_aO is about 64-65% and S_iO_2 is about 20-24% (Kitazume and Terashi, 2013). Three different cement mixing ratios (A_w) of 15, 25, and 35% were adopted to

prepare the samples. Cement-treated soils were prepared using statically compacted stabilized soil technique based on (JGS 0812-2009) before curing. Cement content (C) was determined using the following equation (Kitazume and Terashi, 2013):

$$C = \left\{ \frac{10\rho_t}{\left(\frac{1+w_n}{100}\right)} \right\} \quad [1]$$

where C (kg/m³) is the ratio between the weight of dry cement and the dry weight of soil, while ρ_t and w_n are the wet soil density and the natural water content, respectively.

2.2 Cement-treated soil preparation

Cement-treated soil (CTS) samples were prepared in the laboratory to investigate the mechanical properties of the CTS. Initially, the Ariake clay was sieved through a 425 μ m sieve opening to remove the impurities, insects, and shrubs and ensure the samples' homogeneity. It must be noted that the water content was set as two times the liquid limit of Ariake clay. Under such slurry conditions, the dry mixing method was adopted for soil-cement sample preparation (Kasama et al., 2000).

Therefore, the Ariake clay was mixed adequately with the 15, 25, and 35% dry OPC using an electric hand mixer. The soil-cement samples were then compacted into cylindrical plastic molds (50 mm in diameter and 100 mm in height). The molds were well-sealed to maintain the water content. All the samples were cured at 20 \pm 3°C for 7 and 28 days. Eighteen cured CTS samples varied in the cement content, and the curing period were used for testing. Further details on the sample preparation can be found in (Putera et al., 2021).

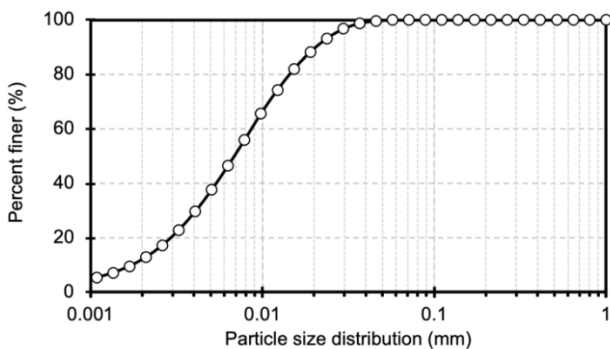


Fig. 1. Ariake Clay particle size distribution curve

2.3 Triaxial testing conditions

Triaxial compression tests were conducted to investigate the mechanical behavior of the CTS samples following the JGS 0523-2009. The tests were loaded under undrained conditions and were isotropically consolidated with 25, 50, and 100 kPa confining pressure (σ_c). The consolidation pressure was applied in this study to reflect the in-situ cement-treated soil at various depths. Since the small-strain range highly depends on the measuring accuracy, a low shearing rate of 0.05 mm/min was applied to ensure reliable results.

In this study, the conventional LDT and LVDTs were used to accurately measure the small and large strain ranges, as delineated in Fig. 3. Moreover, the Axial and Radial LDTs were attached to the samples during testing to determine the Poisson's ratio and the shear modulus. The procedure of attaching the LDTs to a cement-treated soil sample was done following (Putera et al., 2022). Both LDTs were carefully monitored during shearing and were detached from the sample using a hook line from outside the chamber once reaching the maximum displacement capacity.

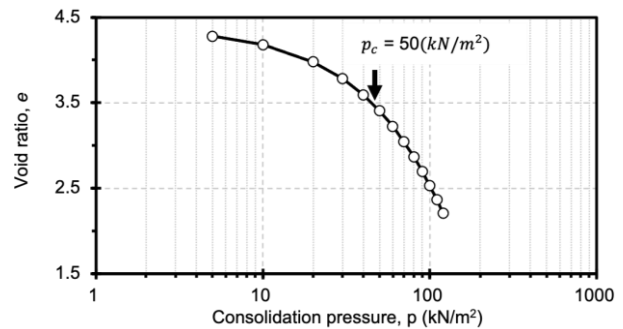


Fig. 2. Ariake clay consolidation curve (e-log p curve)

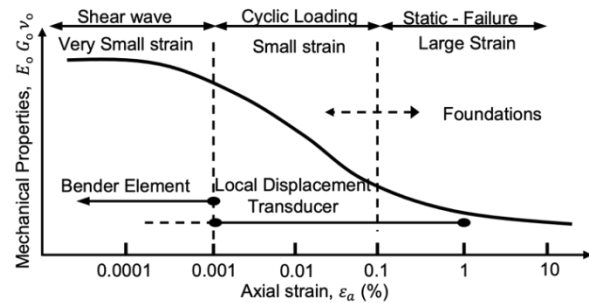


Fig. 3. Typical stiffness variation and variances of strain levels for laboratory tests and structures.

Table 1. Soil Parameter

	Initial Water Content (%)	Soil particle density ρ_s (g/cm ³)	Liquid Limit w_l (%)	Plasticity Index I_P (%)	Compressibility Index C_c	Cement mixing ratios A_w (%)	Cement Content C (kg/m ³)
Ariake clay	232	2.43	100	128.5	2.2	15, 25, 35	55, 92, 128

3. Influence of confining pressure and mechanical behavior in small-strain ranges

The stress-strain relationship of the CTS samples containing 55 and 128 kg/m³ cement content is shown in **Fig. 4**. The axial LDT and LVDT measurements were used to study the mechanical behavior of the CTS within the small-strain ranges. Significant discrepancies were identified in small-strain ranges between LDT and LVDT results for high cement content samples confined at high pressure (100 kPa). Although, low cement content with 25 kPa of confining pressure showed small differences, which might be associated with the low effect of bedding error during loading. Similarly, the discrepancies between the LDT and the LVDT results continue in the large-strain ranges. However, the values tend to converge at high axial strain values.

In the axial-radial strain curves shown in **Fig.4**, small discrepancies were noticed at small-strain ranges for high and low cement content samples confined at low and high pressure. On the other hand, within large-strain ranges, the discrepancies became more significant. Therefore, based on the stress-strain discussion and the results of the axial-radial strain, it can be concluded that using the combination of radial and axial LDT is recommended to determine the strain behavior in the small-strain ranges. Due to the presence of both radial and axial LDT under the same conditions inside the triaxial chamber, the bedding error becomes less significant.

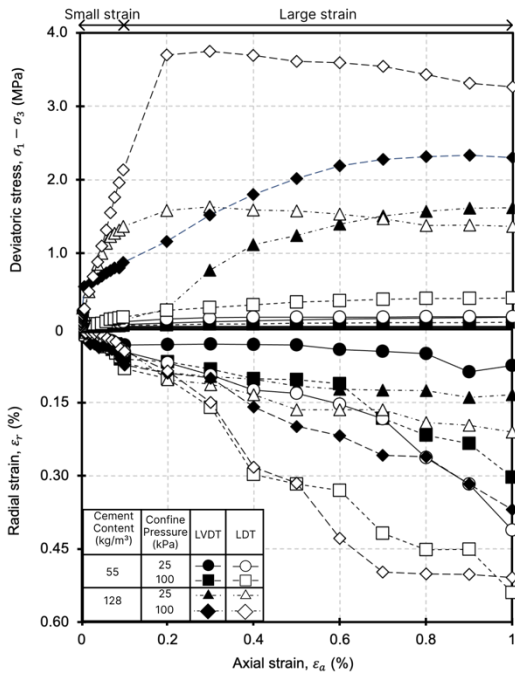


Fig. 4. Stress-strain relationship of cement-treated soils and influence of confining pressure

The discrepancies in the stress-strain curves using different strain measuring devices influences the analyses and the determined values of the small-strain ranges mechanical properties of the CTS. Therefore, to evaluate the discrepancies, the small-strain ranges mechanical properties of the CTS were determined using the secant method (Putera et al., 2022). The degradation of the Initial Young modulus (E_o) using the axial LDT for all the tested samples is shown in **Fig. 5 (a)**. The linear elastic zone for the high and low cement content samples is delineated above each curve. It can be noticed that for low cement content samples, the linear elastic zone extends for higher values within the small-strain range compared to high cement content samples. The axial strain values for the high cement content samples start degrading until it converges to low and almost constant Young modulus values in the large-strain range. **Fig. 5 (b)** compares the measured values using the LDT and LVDT as ratios. It can be noticed that the discrepancies between the measuring devices were more significant in high cement content samples.

Moreover, the Initial Poisson's ratio (ν_o) was determined using the axial and radial LDT for all the tested samples, as shown in **Fig.6**. It must be noted that the higher cement content samples showed lower initial Poisson's ratio values compared to low cement content samples. Moreover, higher confining pressure results in higher values of the initial Poisson's ratio.

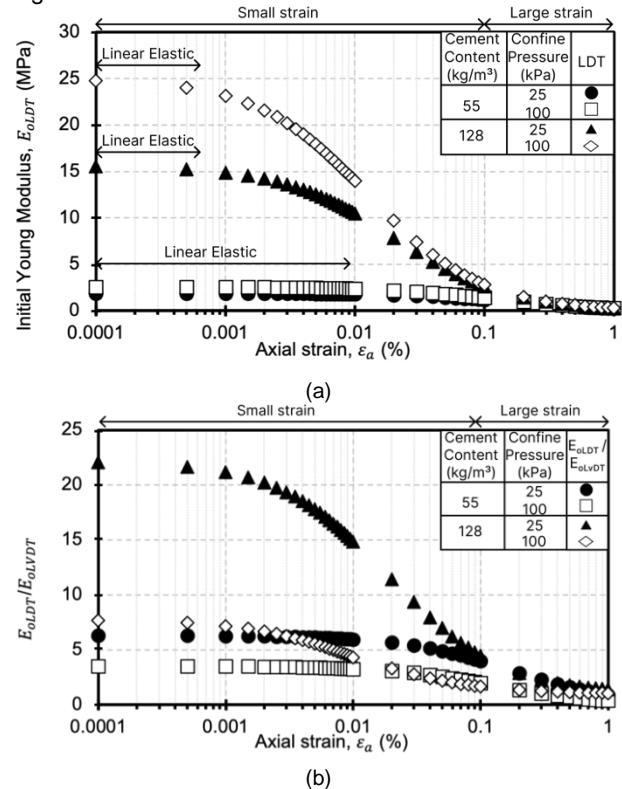


Fig. 5. (a) Degradation of Initial Young Modulus (E_{OLDT}) and (b) Ratio between $E_{OLDT}/(E_{OLVDT})$ with influences of confining pressure.

The young modulus and Poisson's ratio were used to determine and analyze the shear modulus (G_o) within the small-strain ranges, as shown in **Fig. 7 (a)**. While **Fig. 7 (b)** compares the measured values using the LDT and LVDT as ratios. Similar trends of the initial Young's modulus curves were noticed for the Shear modulus at different cement content and confining pressure. Based on the previous discussion, it must be concluded that high degrading values of the mechanical properties occur within the small-strain ranges, which makes it necessary to carefully consider this region, especially when dealing with the elastic settlement.

3.1 Evaluating the relationship between confining pressure and cement content

In order to evaluate the relationship between the confining pressure and the initial mechanical properties, the intercorrelated power function of the confining pressure was used, by applying the following relations:

$$\ln|E_o, v_o, G_o| = \ln \alpha + \beta \ln(\sigma_3/P_a) \quad [2]$$

$$|E_o, v_o, G_o| = \alpha(\sigma_3/P_a)^\beta \quad [3]$$

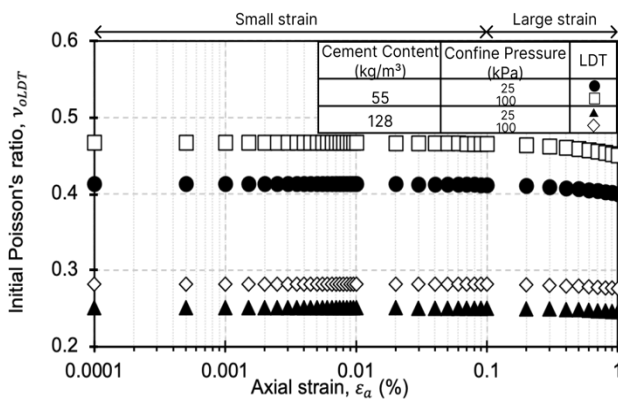
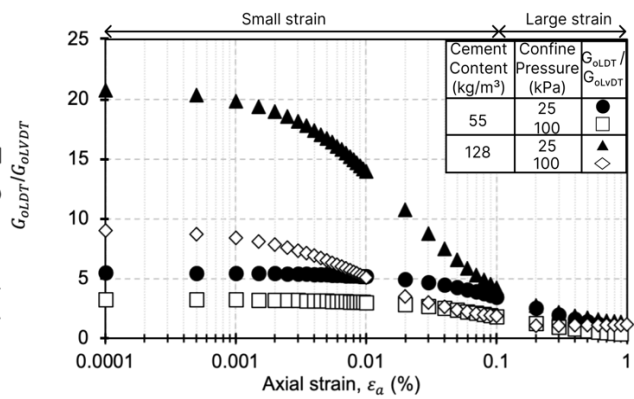


Fig. 6. Degradation of Initial Poisson's ratio (v_{oLDT}) with influences of confining pressure



(b)

Fig. 7. (b) Ratio between $G_{oLDT}/(G_{oLVDT})$ with influences of confining pressure

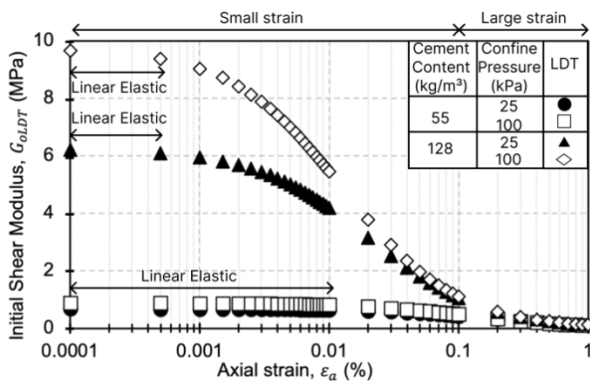


Fig. 7. (a) Degradation of Initial Shear Modulus (G_{oLDT})

where (σ_3/P_a) is the confining pressure normalized with the atmospheric pressure, α is the coefficient parameter concerning the intercorrelation between the cement content and the confining pressure, while β is the slope rate of the coefficient parameter between differences of cement content and confining pressure.

The variation of logarithm of Initial young modulus (E_o/P_a) against (σ_3/P_a) were plotted in **Fig. 8**. It can be noticed that low cement content samples showed large discrepancies values within the small-strain range compared to high cement content samples. It was shown that the power function showed a good relation for all the samples at different cement content, confining pressure, and curing period. However, the initial Poisson ratio (v_o) has been shown in **Fig. 9** the different order of curve relationship. It must be noted that the higher cement content samples showed lower initial Poisson's ratio values compared to low cement content samples. A sufficiently low increment of stiffness is the lowest cement content on CTS. Contrary, in **Fig. 10**, the increment of curing days on Initial Poisson's ratio was described as significant discrepancies, especially at the highest and lowest cement content. While, Similar trends of the initial Young's modulus curves were noticed for the Shear modulus at different cement content and confining pressure.

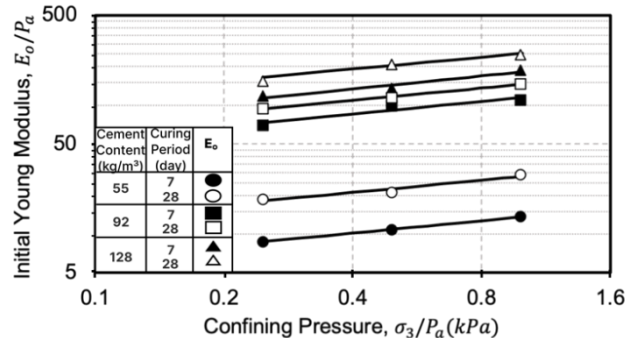


Fig. 8. Initial Young Modulus (E_o/P_a) and confining pressure (σ_3/P_a) in small-strain ranges

Therefore, based on the previous discussion, the effect of the confining pressure in small-strain ranges confirms the significant relationship with the increment of the coefficient parameters (α) and (β) with the initial mechanical properties, which can be used for predicting the elastic settlement as discussed in section 4.

4. Elastic settlement of cement-treated soils in small-strain ranges

Researchers commonly adopt the following formula to determine the elastic settlement (S_e) for a shallow foundation structure:

$$S_e = qB \frac{1 - \nu_{soil}}{E_{soil}} I \quad [4]$$

The model considers three main parameters. The loading parameter; q is the applied stress. The geometry parameters; B is the diameter of the foundation and I is the influence factor reflecting the footing shape. And the soil properties parameters, where E_{soil} and ν_{soil} are Young's modulus and Poisson's ratio of the underlying natural ground, respectively. Based on Poulos (1968), for circular rigid geometry, the influence factor is assumed to be 1, although the flexible geometry was considered $\pi/4$. Das (1985) reported that for a square footing, the factor is estimated using the ratio between the length and width of the rectangular geometry. However, a definite way of estimating the shape parameter for cement-treated shallow soil profile is lacking.

4.1 Equivalent geometry of a shallow rectangular stabilization

A simple soil profile unit is adopted in this study to estimate the elastic settlement of CTS, considering the wheel-base position as illustrated in Fig. 11. Initially, the most severe case is considered, which is associated with the highest axial load due to the wheel-base position of the HSR (Jeon et al. 2015; Hu et al. 2015).

The circular geometry equation of elastic settlement is generally used to estimate the equivalent rectangular shape factor under uniform loading (Horikoshi, 1997; Mayne, 1999), which can be expressed as follows:

$$B_{CTS} = \left(\frac{4BL}{\pi} \right)^{0.5} ; a = 0.5B_{CTS} \quad [5]$$

where B_{CTS} is equivalent to the cross-section breadth of the CTS rectangular geometry based on the wheel-base position, while B is the section breadth and L is the section length, as can be seen in Fig. 11. While a is half of the B_{CTS} . Those equivalents were used to determine the ratios between the equivalent section breadth (B_{CTS}) and the section length (L), where B_{CTS} is longer than L , as follows:

$$b = \left(\frac{B_{CTS}}{L} \right) \quad [6]$$

where b is the aspect ratio of the section breadth and length of CTS geometry. Therefore, b is a valuable parameter that defines the equivalent of the rectangular geometry of the CTS that can be used to predict the elastic settlement in the HSR projects. In addition, it would be applied to evaluate the influence factor and dynamic load on the shallow stabilization layer.

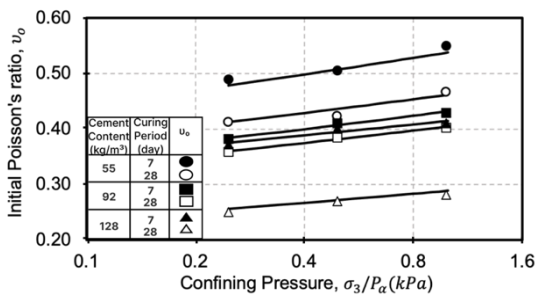


Fig. 9. Initial Poisson's ratio (ν_0) and confining pressure (σ_3/P_a) in small-strain ranges

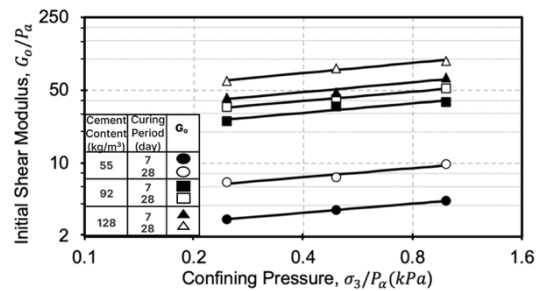


Fig. 10. Initial Shear modulus (G_0/P_a) and confining pressure (σ_3/P_a) in small-strain ranges

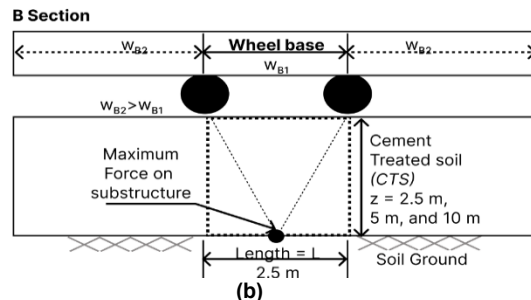
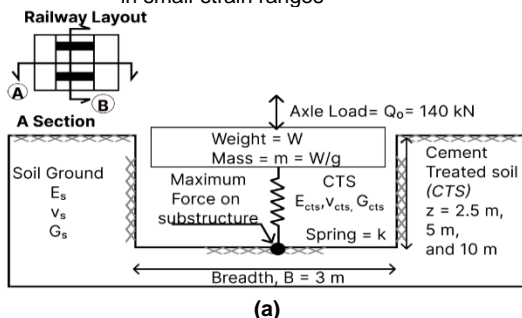


Fig. 11. Illustration of CTS boundaries condition for dynamic load behaviors from wheel-base (a) Cross Section (b) Long section

4.2 Maximum dynamic load on shallow stabilization

The railway substructure has advantages in reducing the stress caused by transmitted axle and dynamic loading from the train (Lazorenko et al., 2019). In this research, the dynamic properties of the CTS were studied in small-strain ranges to evaluate and analyze the critical condition of load transmission through the ground. The Boussinesq formula, Eq. 4, only considers the static loading for homogeneous soil layers (Hu et al., 2016). However, evaluating the CTS under dynamic loading is still lacking. In this study, the spring-mass system of rectangular geometry proposed by Worku (2017) was used to consider the dynamic loading under the CTS. The spring-mass function can be expressed as follows:

$$k_v = \frac{4 \cdot G \cdot B}{1 - \nu} \quad [7]$$

where k_v is the vertical spring-mass system of a circular soil layer geometry, while B is its breadth. G and ν are the shear modulus and Poisson's ratio of the soil. In order to determine the equivalent geometry of the rectangular CTS, the following formula can be used:

$$k_{CTS} = \frac{G_{CTS} \cdot B_{CTS} \cdot b}{1 - \nu_{CTS}} \quad [8]$$

where k_{CTS} is the vertical spring-mass system of the equivalent geometry of the rectangular CTS, while b is the aspect ratio of the section breadth and length of CTS geometry. Therefore, the dynamic parameters of CTS

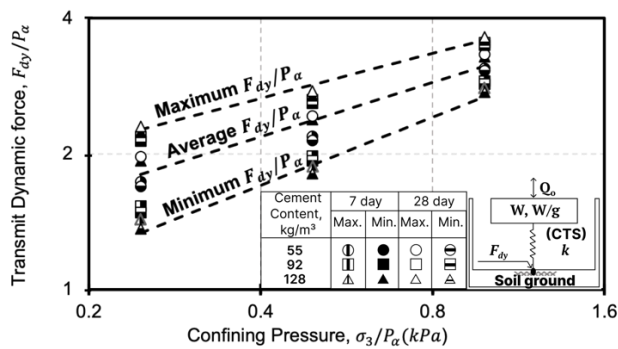


Fig. 12. Force vibration of a mass-spring system on CTS related to the confining pressure (σ_3/P_a).

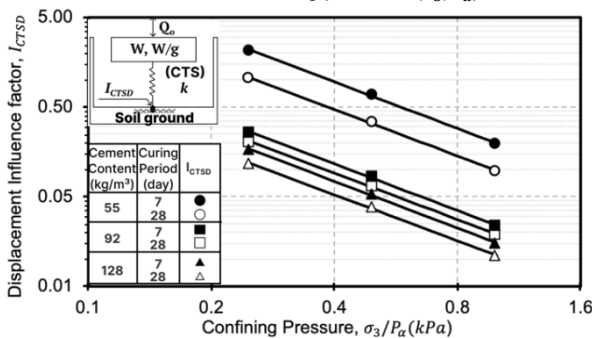


Fig. 14. Effect of Displacement Influence factor (I_{CTS}) of CTS related to the confining pressure (σ_3/P_a).

were defined by the shear modulus (G_{CTS}) and Poisson ratio (ν_{CTS}). The k_{CTS} under the natural response of CTS loading can be determined using the natural angular frequency (ω_n) as shown below:

$$\omega_n = \sqrt{\frac{k_{CTS}}{m}} \quad [9]$$

where ω_n indicates the natural vertical vibration movement of the CTS above the natural soil ground. While m is the mass of the CTS, and it can be calculated using its volume and density. In order to consider the dynamic force of the CTS caused by the train movement, the angular frequency from train loading to the ground (ω) can be determined as follows (Soomro, 2019):

$$\omega = 2 \cdot \pi \cdot f_{train} \quad [10]$$

where f_{train} is the frequency applied by the train. Generally, the vibrational frequency for clayey soils has been evaluated between 11 and 25 Hz (Lazorenko et al., 2019). However, Jones (1994) confirmed that for the HSR and considering the wheel-base length (L), f_{train} equals to 11 Hz. Consequently, the dynamic force from the HSR train under CTS can be delineated as follow:

$$F_{dy} = W \pm \frac{Q_o}{1 - \omega/\omega_n} \quad [11]$$

where W is the total mass of the CTS structures, while the Q_o is the point load of the HSR train wheel-base distribution. This study adopted 140 kN stress above the natural ground representing the 2.5 m length of the wheel-base (Hu et al., 2016).

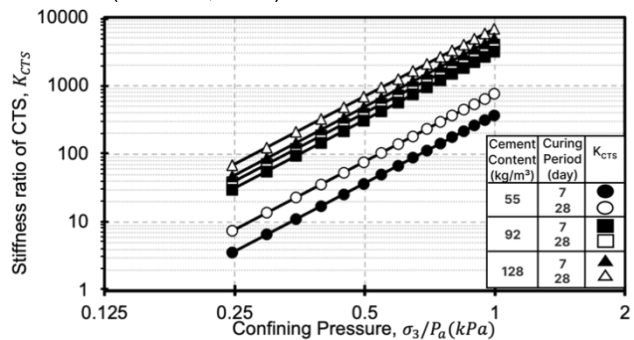


Fig. 13. (a) Effect of foundation flexibility factor (K_{CTS}) of CTS related to the confining pressure (σ_3/P_a).

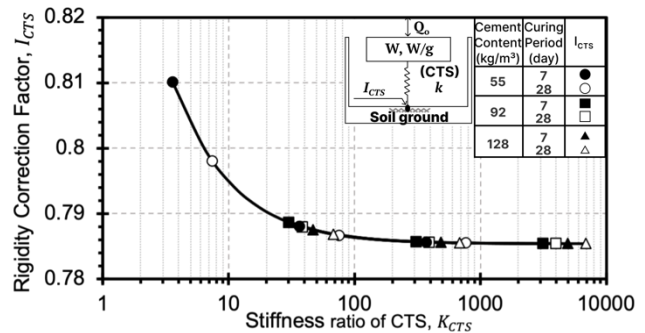


Fig. 15. (b) Effect of cement-treated soil rigidity correction factor (I_{CTS}) associated with Foundation Flexibility Factor (K_{CTS})

The relationship between the maximum and minimum dynamic force transmitted to the reference point and the confining pressure is illustrated in **Fig. 12** for all the CTS samples with different cement content and curing period. It can be noticed that different confining pressures result in different dynamic force values, with the high cement content at a high curing period attaining the highest values. It must be noted that the values of the dynamic force showed smaller ranges at high confining pressures compared to those at low confining pressures where the CTS reached high stiffness. Based on this discussion, the dynamic force can be evaluated using the power function to determine the relationship with the normalized confining pressure, as shown below:

$$F_{dy} = \alpha(\sigma_3/P_a)^\beta \quad [12]$$

where α and β are the coefficient parameters concerning the intercorrelation between the dynamic loading and the confining pressure.

4.3 Displacement Influence factor of cement-treated soils layer

The displacement influence factor was considered by vertical deflection beneath the substructure within the dynamic load. The maximum displacement at the reference point was evaluated by the thickness of the CTS layer. Poulos and Davis (1968) and Mayne and Poulos (1999) mentioned the general derivation for the influence of the vertical displacement on natural soil ground. In this research, for the CTS under dynamic loading, the equations were derived as follows:

$$\frac{\sigma_z}{F_{dy}} = 1 - \left[1 + \left(\frac{b}{z} \right)^2 \right]^{-1.5} \quad [13]$$

$$\frac{\sigma_r}{F_{dy}} = \frac{1}{2} (1 + 2\nu_{CTS}) - (1 + \nu_{CTS}) \left[\left(\frac{b}{z} \right)^2 + 1 \right]^{0.5} + \frac{1}{2} \left[\left(\frac{b}{z} \right)^2 + 1 \right]^{-1.5} \quad [14]$$

where σ_z/F_{dy} is the ratio between the vertical stress and the axial dynamic loading, σ_r/F_{dy} is the ratio between the radial stress and the axial dynamic loading, where b was used to represent the equivalent of the radial dimension. While z is the thickness of the CTS. Therefore, the vertical displacement (ΔI_z) and the influence displacement factor of CTS (I_{CTSD}) can be determined as follows:

$$\Delta I_z = \left(\frac{1}{E_{CTS}} \right) (\Delta \sigma_z + 2\nu_{CTS} \Delta \sigma_r) \quad [15]$$

$$I_{CTSD} = \sum \Delta I_z \cdot (\Delta z/b) \quad [16]$$

Furthermore, to validate the CTS thickness layer with the I_{CTSD} at certain depths, the relationship between the I_{CTSD} and the confining pressure is illustrated in **Fig. 13** for all the CTS samples with different cement content and curing period. Based on the results, the influence factor tends to decrease with the increase of the confining pressure. This behavior confirms the high influence of the CTS layer thickness on the displacement. Moreover, high cement content, 128 and 92 kg/m³, showed values of the influence displacement factor of less than 1 for under confining pressures, reducing the settlement behavior. On the other hand, low cement content results in high influence displacement factor values, which mean higher vertical displacement for shallow and deep stabilization.

Based on this discussion, the influence displacement factor can be evaluated using the power function to determine the relationship with the normalized confining pressure, as shown below:

$$I_{CTSD} = \alpha(\sigma_3/P_a)^\beta \quad [17]$$

where α and β are the coefficient parameters concerning the intercorrelation between the influence displacement factor and the confining pressure.

4.4 Rigidity correction factor related to stiffness ratio cement-treated soils

The increasing rigidity of the CTS layer indicates how properly the cement content has improved the natural ground. As discussed in section 3, both the curing period and cement content significantly influence the mechanical properties of CTS in small-strain ranges. Therefore, in this study, the rigidity correction factor was determined to optimize the elastic settlement prediction for CTS.

By referring to the classification of rigidity in shallow reinforcement structure, the influence foundation flexibility factor is calculated using the equation below (Horikoshi and Randolph, 1997; Mayne and Poulos, 1999):

$$K_F = \left(\frac{E_F}{E_S} \right) \left(\frac{z}{a} \right)^3 \quad [18]$$

where the K_F is the foundation flexibility factor, the initial form is derived with stiffness ratios between the structure and the soil. While E_F and E_S are Young's modulus of the foundation and the soil, respectively. In order to determine the foundation flexibility factor for the CTS, its mechanical properties and thickness layer must be considered. Therefore, the stiffness ratio of the CTS (K_{CTS}) can be determined as follows:

$$K_{CTS} = b \left(\frac{E_{CTS}}{E_S} \right) \left(\frac{z}{B_{CTS}} \right)^3 \quad [19]$$

Fig. 14 (a) shows the relationship between K_{CTS} and σ_3/P_a . The results present steep curves on the logarithm scale. The stiffness ratio showed higher values for the 128 and 92 kg/m³ than the 55 kg/m³ cement content samples. The relationship with the normalized confining pressure can be evaluated using the power function as shown below:

$$K_{CTS} = \alpha(\sigma_3/P_a)^\beta \quad [20]$$

where α and β are the coefficient parameters concerning the intercorrelation between the stiffness ratio and the confining pressure

Using the stiffness ratio of the CTS, the rigidity correction factor (I_{CTS}) can be determined as follows (Mayne and Poulos, 1999):

$$I_{CTS} = \frac{\pi}{4} + \frac{1}{(4.6 + 10 K_{CTS})} \quad [21]$$

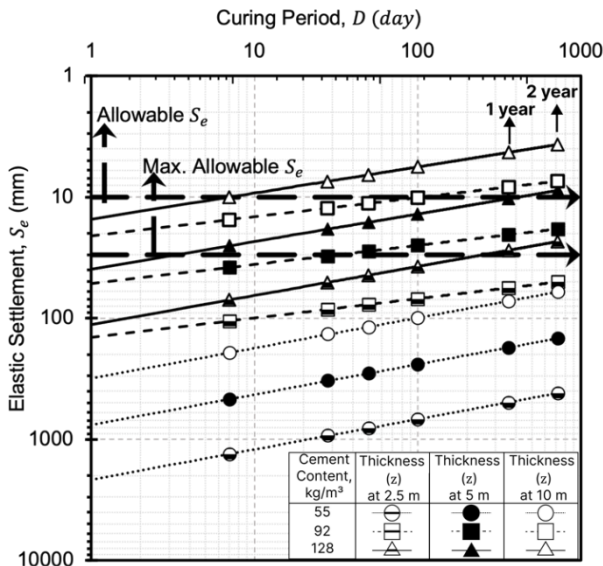


Fig. 16. Elastic settlement of CTS with curing period based on rigidity correction factor (I_{CTS}) and Displacement Influence factor ($I_{CTS D}$).

In previous research, the relationship between the foundation flexibility factor and the stiffness ratio was defined by a curvature slope, and by solving the analytical solutions, I was found to be 1 and $\frac{\pi}{4}$ for the perfectly rigid and flexible foundations, respectively. Using Eqs. 20 and 21, the relationship between K_{CTS} and I_{CTS} was delineated as shown in **Fig. 14 (b)**. For low cement content, 55 kg/m³, the values of the I_{CTS} were very high compared with the high cement content samples, 92 and 128 kg/m³, which means they became rigid structures, especially with increasing the curing period. However, low cement content might cause high vertical displacement due to the lack of stiffness and low strength.

4.5 Elastic Settlement prediction of cement-treated soils subjected to curing time in small-strain ranges

Using the defined Boussinesq formula and the modified parameters related to the dynamic loading, the geometry and the parameters of the CTS under small-strain ranges, and the soil properties, the newly proposed model to predict the elastic settlement for CTS (S_{eCTS}) can be delineated as follows:

$$S_{eCTS} = F_{dy} \cdot B_{CTS} \cdot \frac{1 - \nu_{soil}^2}{E_{soil}} I_{CTS D} I_{CTS} \quad [22]$$

The model considers the CTS's cement content, curing period, and thickness layer, making it a reliable solution to determine the elastic settlement for various projects.

Considering the settlement at different times during construction and operation, estimating the settlements using a simple interpolation formula is essential. Previous research estimated the time-dependent settlement by proposing a simple power function formula of the relation between cement content and mechanical properties (Kang et al., 2017). Commonly, the construction period ends within at least a year; however, the serviceability phase afterward should be considered.

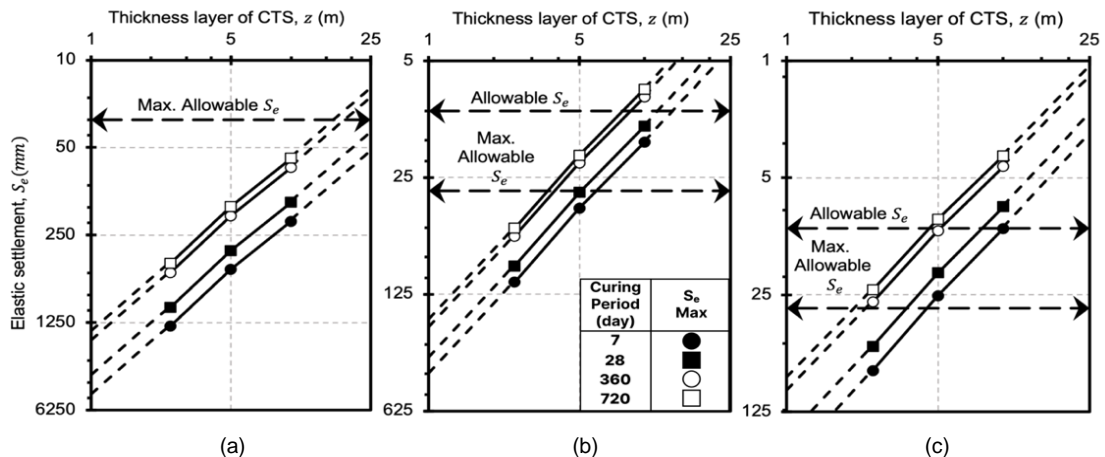


Fig. 17. Elastic settlement of CTS (S_e) vs thickness of CTS (z) with (a) 55 kg/m³, (b) 92 kg/m³ and (c) 128 kg/m³ of cement content under small strain ranges and maximum of Dynamic forces

Fig. 15 shows the relationship between the elastic settlement and the curing period delineating the variation in the cement content and the CTS's thickness. For 55 kg/m³ that can be noticed all the time-dependent of curing period, the elastic settlement exceeds the maximum allowable value. Therefore, It can be noticed that for a year curing period, for 92 kg/m³ and 128 kg/m³ of the cement content samples does not exceeds the maximum allowable value. Moreover, when increasing the cement content from 92 kg/m³ to 128 kg/m³ with similar CTS's thickness (5 m), the elastic settlement prediction does not exceed the maximum allowable settlement within 7 days of curing periods.

4.6 Elastic Settlement prediction of cement-treated soils subjected to thickness layer in small-strain ranges

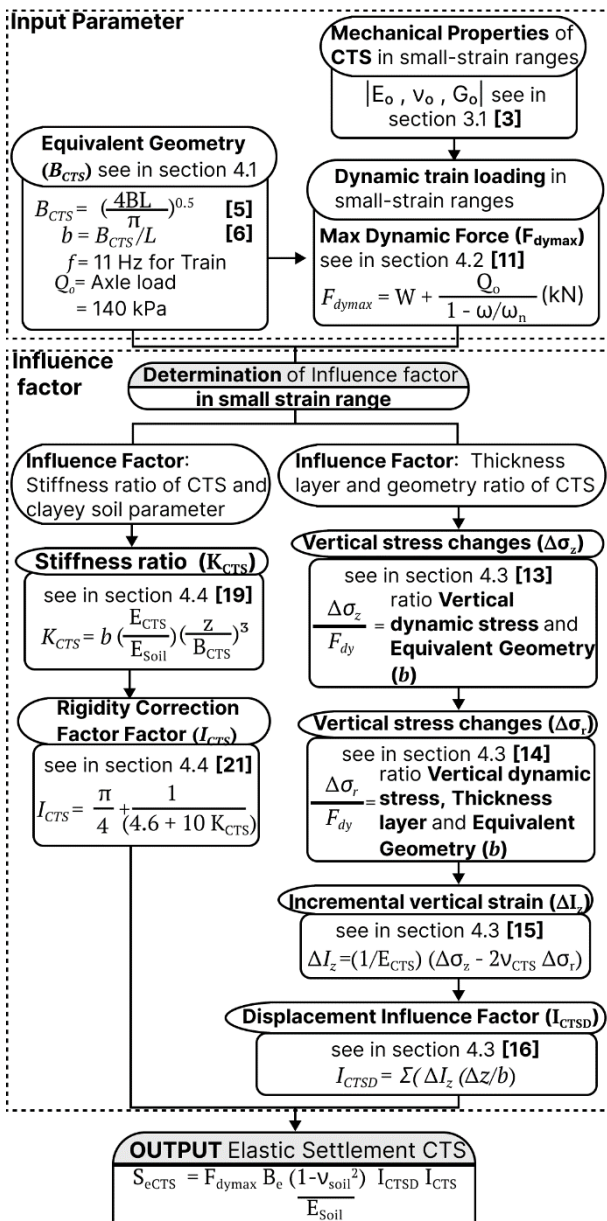


Fig. 18. Elastic Settlement of CTS (S_e) determination process reflecting to the result from small strain measurement.

The proposed model and results were further analyzed to predict the elastic settlement based on the thickness of the CTS layer. However, obtaining an optimum design related to the thickness layer is applicable by comparing various cement amount parameters. Therefore, various thicknesses were used to study the relationship between the elastic settlement and the thickness layer. Using the power function, the following formula can be delineated:

$$S_{eCTS} = \alpha(z)^\beta \quad [23]$$

where α and β are the coefficient parameters concerning the intercorrelation between the cement content and the curing period. Fig. 16 (a) shows the elastic settlement behavior for 55 kg/m³ of cement content samples at different thickness layers. It can be noticed that for all the thicknesses, the elastic settlement exceeds the maximum allowable value. Therefore, a suitable combination of ground improvement with deep mixing or group column type reinforcement is required to reduce the settlement in low cement content treated- soil. Fig. 16 (b) delineated the elastic settlement behavior for 92 kg/m³ cement content samples. For a CTS thickness of 5 m, the predicted elastic settlement after 1-2 years does not exceed the maximum allowable settlement. However, for a CTS thickness of 10 m, the predicted elastic settlement does not exceed the maximum allowable settlement despite the curing period. Moreover, when increasing the cement content, despite the curing period and the CTS's thickness, the elastic settlement does not exceed the maximum allowable settlement, as illustrated in Fig. 16 (c).

Fig. 17 illustrates the determination process of S_e considering the thickness layer of CTS, curing period, and the maximum dynamic forces. The input parameters account for the CTS mechanical behaviors in small-strain ranges that can be easily determined using triaxial undrained testing. The maximum dynamic forces can be determined by substituting the equivalent dimensions parameter of the CTS layer and applying the vertical spring system. Consequently, influence factors I_{CTS} and I_{CTSD} can be determined. The newly proposed model enhanced the prediction method by considering CTS's thickness and the curing period. However, the model needs to be extended to predict bigger ranges of curing periods, especially for long-term serviceability phases and estimating the maintenance periods.

5. Conclusions

Through this paper, the mechanical characteristics of cement-treated clayey soil underlying a high-speed train railway were experimentally investigated to elaborate on

the elastic settlement behavior, considering the influence of the curing period, cement content, and the confining pressure. Focusing on the small-strain ranges, a series of triaxial undrained testing equipped with local displacement transducers (*LDT*) was carried out to optimize the cement mixing ratio and curing time aiming at suppressing the elastic settlement within the standard requirements. Furthermore, a model was proposed to estimate the settlement of cement-treated clayey soil. The main findings of this study can be outlined as follows:

1. A simple power formula that captures the initial mechanical properties parameters (Young's modulus, Poisson's ratio, shear modulus) as a function of the confining pressure, cement content, and curing periods was proposed. It was found that the Young's and shear moduli for a straight line on a log-log scale versus the cement content and confining pressure.
2. A simple elastic settlement prediction model was proposed for cement-treated clayey soil subjected to dynamic loading (high-speed train), focusing mainly on the small-strain range. The model included three main factors to reflect the applied dynamic force (F_{dyn}), displacement influence factor (I_{CTSD}) and rigidity correction factor (I_{CTS}). A power formula was empirically introduced to express the new factors as a function of the confining pressure and the thickness of the cement-treated soil layer. The model can estimate the time-dependent elastic settlement of cement-treated soils based on the measured small-strain mechanical properties of at least two curing periods, assuming an extrapolation using the proposed power formula.
3. The prediction model optimized the mixing ratio at a specific curing period, reflecting the wheel-base loading on the cement-treated soil layer. For example, using Ariake clay, subjected to a dynamic loading of 140 kN force spanning over 2.5 m wheel-base, the elastic settlement can be minimized using high cement content $> 100 \text{ kg/m}^3$. While the curing period should not be less than 100 days to ensure achieving the aimed hardening of the cement.

Acknowledgements

The authors express their gratitude to the laboratory technical assistant Mr. Michio Nakashima for their great support.

References

- Ando, K., Sunaga, M., Aoki, H., Haga, O., 2021. Development of slab tracks for hokuriku shinkansen line. Quarterly Report of RTRI 42, 35–41.
- Atkinson, J., 2000. Non-linear soil stiffness in routine design. *Geotechnique* 50, 487–508. <https://doi.org/10.1680/geot.2000.50.5.487>
- Das, B.M., 1985. *Advanced soil mechanics*. McGraw-Hill, New York.
- Das, B.M., Ramana, G.V., 2010. *Principles of soil dynamics*, Second edition. ed. CL Engineering.
- Fang, H.-Y., Daniels, J.L., 2006. *Introductory Geotechnical Engineering: An Environmental Perspective (1st ed.)*, 1st ed. CRC Press, London.
- Firoozi, Ali Akbar, Guney Olgun, C., Firoozi, Ali Asghar, Baghini, M.S., 2017. Fundamentals of soil stabilization. *International Journal of Geo-Engineering* 8, 26. <https://doi.org/10.1186/s40703-017-0064-9>
- Foye, K.C., Basu, P., Prezzi, M., 2008. Immediate Settlement of Shallow Foundations Bearing on Clay. *international Journal of Geomechanics* 8, 300–310. [https://doi.org/10.1061/\(ASCE\)1532-3641\(2008\)8:5\(300](https://doi.org/10.1061/(ASCE)1532-3641(2008)8:5(300)
- Horikoshi, K., Randolph, M.F., 1997. On the definition of raft—soil stiffness ratio for rectangular rafts. *Géotechnique* 47, 1055–1061. <https://doi.org/10.1680/geot.1997.47.5.1055>
- Hu, J., Bian, X., Jiang, J., 2016. Critical Velocity of High-speed Train Running on Soft Soil and Induced Dynamic Soil Response. *Procedia Engineering* 143, 1034–1042. <https://doi.org/10.1016/j.proeng.2016.06.102>
- Ikeagwuani, C.C., Nwonu, D.C., Obetule, D.A., Omeje, M.U., Festus, T., 2019. Potential of bamboo stem ash as supplementary cementitious material in concrete production. *International Journal of Engineering Research & Technology (IJERT)* 08, 75–80.
- JETRO, 2012. Study on the high speed railway project (jakarta-bandung section), republic of indonesia (Final report (Summary)), Feasibility study for promotion of international infrastructure projects in fy2011. Yachiyo Engineering Co., Ltd. and Japan International Consultants for Transportation Co., Ltd.
- Kanazawa, H., Tarumi, H., 2010. Technical transition of earth structures for shinkansen. *SOILS AND FOUNDATIONS* 50, 817–828. <https://doi.org/10.3208/sandf.50.817>
- Kang, G., 2016. Influence and Control Strategy for Local Settlement for High-Speed Railway Infrastructure. *Engineering* 2, 374–379. <https://doi.org/10.1016/J.ENG.2016.03.014>

- Kang, G., Tsuchida, T., Kim, Y., 2017. Strength and stiffness of cement-treated marine dredged clay at various curing stages. *Construction and Building Materials* 132, 71–84.
<https://doi.org/10.1016/j.conbuildmat.2016.11.124>
- Kasama, K., Ochiai, H., Yasufuku, N., 2000. On the Stress-Strain Behaviour of Lightly Cemented Clay Based on an Extended Critical State Concept. *Soils and Foundations* 40, 37–47.
https://doi.org/10.3208/sandf.40.5_37
- Kitazume, M., Terashi, M., 2013. The deep mixing method, in: *The Deep Mixing Method*. CRC Press/Balkema, Leiden, The Netherlands.
- Kumar, P., Singh, V., 2017. Geotechnical Aspect for Design of Track Formation System for High Speed Rail Lines on Alluvial Soil Deposited-A Review.
- Lazorenko, G., Kasprzhitskii, A., Khakiev, Z., Yavna, V., 2019. Dynamic behavior and stability of soil foundation in heavy haul railway tracks: A review. *Construction and Building Materials* 205, 111–136.
<https://doi.org/10.1016/j.conbuildmat.2019.01.184>
- Mayne, P., Poulos, H., 1999. Approximate Displacement Influence Factors for Elastic Shallow Foundations. *Journal of Geotechnical and Geoenvironmental Engineering - J GEOTECH GEOENVIRON ENG* 125.
[https://doi.org/10.1061/\(ASCE\)1090-0241\(1999\)125:6\(453\)](https://doi.org/10.1061/(ASCE)1090-0241(1999)125:6(453))
- Novico, F., Menier, D., Mathew, M., Ramkumar, M., Santosh, M., Endyana, C., Dewi, K.T., Kurniawan, I., Lambert, C., Goubert, E., Hendarmawan, 2022. Impact of Late Quaternary climatic fluctuations on coastal systems: Evidence from high-resolution geophysical, sedimentological and geochronological data from the Java Island. *Marine and Petroleum Geology* 136, 105399.
<https://doi.org/10.1016/j.marpetgeo.2021.105399>
- Pantelidis, L., Gravanis, E., 2020. Elastic Settlement Analysis of Rigid Rectangular Footings on Sands and Clays. *Geosciences* 10.
<https://doi.org/10.3390/geosciences10120491>
- Poulos, H., Davis, E., 1968. The Use of Elastic Theory for Settlement Prediction Under Three-Dimensional Conditions. *Geotechnique* 18, 67–91.
<https://doi.org/10.1680/geot.1968.18.1.67>
- Putera, M.A., Yasufuku, N., Alowaisy, A., Ishikura, R., Hussary, J.G., Rifa'i, A., 2022. Evaluating the small-strain mechanical properties of cement-treated clayey soils based on the confining pressure. (Accepted).
- Putera, M.A., Yasufuku, N., Alowaisy, A., Rifai, A., 2021. Optimizing modified triaxial testing for small strain zone using local displacement transducers and bender element for cement-treated soft soil. *E3S Web of Conferences* 331.
<https://doi.org/10.1051/e3sconf/202133103003>
- Ranst, E.V., Utami, S.R., Vanderdeelen, J., Shamshuddin, J., 2004. Surface reactivity of Andisols on volcanic ash along the Sunda arc crossing Java Island, Indonesia. *Geoderma* 123, 193–203.
<https://doi.org/10.1016/j.geoderma.2004.02.005>
- Razouki, S.S., Al-Zubaidy, D.A., 2010. Elastic settlement of square footings on a two-layer deposit. *Proceedings of the Institution of Civil Engineers - Geotechnical Engineering* 163, 101–106.
<https://doi.org/10.1680/geng.2010.163.2.101>
- Skempton, A.W., Bjerrum, L., 1957. A contribution to the settlement analysis of foundations on clay. *Géotechnique* 7, 168–178.
<http://dx.doi.org/10.1680/geot.1957.7.4.168>
- Soomro, Z.A., 2019. Analysis for angular velocity of railway wheelset measurement and creep error estimation. *International Robotics & Automation Journal* 5, 63–67.
<https://doi.org/10.15406/iratj.2019.05.00175>
- Worku, A., 2017. The use of springs in static analysis of structures to account for short-and long term subgrade deformations. *Journal of Experimental Aircraft Association* 24.

Symbols and abbreviations

α	Coefficient parameter of cement-treated soils
a	Half rectangular geometry
A_w	Soil-cement percentage
β	Coefficient parameter of cement-treated soils
B	Diameter of circle foundation
B_{CTS}	Equivalent of breadth of structure geometry
b	Aspect ratio breadth and length
C	Cement amount
E_o and E_{CTS}	Initial young modulus of cement treated soils
F_{dy}	Dynamic force based on train loading
f_{train}	Frequency of train loading
G_o and G_{CTS}	Initial shear modulus of cement treated soils
HSR	High-speed railway
I	Influence of the shape factor

I_{CTS}	Rigidity correction factor of cement-treated soils
I_{CTSD}	Displacement influence factor of cement-treated soils
I_z	Incremental vertical strain
K_{CTS}	Stiffness factor of cement-treated soils
K_F	Foundation flexibility factor
k_v	Vertical spring mass system
k_{CTS}	Vertical spring mass system of CTS rectangular shape
LDT	Local displacement transducer
LVDT	Linear variable differential transformer
L_{CTS} and L	Actual length of rectangular shape geometry
m	Mass of cement-treated soils
P_a	Atmospheric pressure = 101.4 kPa
q	Applied stress
S_e	Elastic settlement of soil
S_{eCTS}	Elastic settlement of cement-treated soils
w_n	Natural water content
z	Thickness layer or depth of embedment structures.
ρ_t	Soil density
σ_3 and σ_c	Confining pressure
ω_n	Natural angular frequency
ω	Angular frequency
σ_z	Vertical stress changes
σ_r	Vertical stress changes with thickness layer